crystals

MDPI

Article

Time-Dependent Evolution of Nanostructure Formation on CdI_2 Crystal Surfaces

Ivan Rovetskii [1], Halyna Klym [2], Ivan Karbovnyk [3,*], Marina Konuhova [4], Nadezda Kongi [5] and Anatoli I. Popov [4,6,7,*]

1 Department of Information Technologies and Electronic Communication Systems, Lviv State University of Life Safety, Kleparivska Str., 35, 79007 Lviv, Ukraine; rovetskii.ivan@gmail.com
2 Department of Specialized Computer Systems, Institute of Computer Technologies, Automation and Metrology, Lviv Polytechnic National University, 12 Bandera Str., 79013 Lviv, Ukraine; halyna.i.klym@lpnu.ua
3 Department of Radiophysics and Computer Technologies, Faculty of Electronics and Computer Technologies, Ivan Franko National University of Lviv, 50, Dragomanova Str., 79005 Lviv, Ukraine
4 Institute for Solid State Physics, University of Latvia, Kengaraga 8, LV-1063 Riga, Latvia; marina.konuhova@cfi.lu.lv
5 Institute of Chemistry, University of Tartu, Ravila 14A, 50411 Tartu, Estonia; nadezda.kongi@ut.ee
6 School of Integrated Circuits and Chongqing University of Posts and Telecommunications Innovation Institute, Chongqing University of Posts and Telecommunications, Chongqing 400065, China
7 Department of Technical Physics, Institute of Physics and Technology, L.N. Gumilyov Eurasian National University, Kazhymukan St. 13, Astana 010008, Kazakhstan
* Correspondence: ivan.karbovnyk@lnu.edu.ua (I.K.); popov@latnet.lv (A.I.P.)

Abstract

The time evolution of nanoscale structure formation on the surface of CdI_2 crystals grown both from the melt and from the gas phase is investigated. Atomic force microscopy was used to show that, already at the initial stages of exposure to air at room temperature, island-shaped nanostructures form, which subsequently aggregate into nanoclusters as the exposure time increases. Similar nanostructures, including nanopores and nanoclusters, are observed for CdI_2 crystals grown from the gas phase after prolonged exposure to air. Photoluminescence spectroscopy indicates that the formed nanoclusters are consistent with the presence of cadmium hydroxide ($Cd(OH)_2$) and cadmium oxide (CdO). The formation of nanostructures determines the time evolution of the low-temperature luminescence spectra of CdI_2 crystals. Additional bands with maxima at 1.87 eV and long-wavelength luminescence in the region with a maximum at 1.68 eV appear in the spectral structure. These results highlight the close relationship between surface structural evolution and the time-dependent optical properties of CdI_2.

Keywords: atomic force microscopy; CdI_2 crystals; surface; nanostructures; nanoclusters; luminescence spectra

Academic Editors: Ljubica Đačanin Far and Tamara V. Gavrilović

Received: 18 January 2026
Revised: 13 February 2026
Accepted: 17 February 2026
Published: 22 February 2026

1. Introduction

Alkali and alkaline-earth halides continue to attract significant scientific interest due to their fundamental role in solid-state physics, materials chemistry, and photonic technologies [1–3]. These compounds exhibit a wide range of optical, luminescent, and electronic properties that make them valuable in radiation detection, scintillation, photonics, and optoelectronic devices [4–18].

Among them, cadmium iodide (CdI_2) is a highly significant layered halide material with widespread applications in optoelectronics and photonics. Its strong transparency

in the visible range, favorable nonlinear optical characteristics, and pronounced excitonic behavior make it attractive for various optical and electronic devices [19–24]. The material's strongly anisotropic layered structure also renders its surface highly sensitive to environmental effects. When exposed to atmospheric conditions, CdI_2 undergoes structural modifications that promote the spontaneous formation of surface nanostructures, which can substantially alter its physical, optical, and luminescent properties [23–28].

A major research focus is the elucidation of nanostructure formation mechanisms on CdI_2 crystal surfaces and their influence on the material's luminescence characteristics and defect-related properties [29–31]. Owing to its tunable band gap, pronounced excitonic response, and capacity for impurity incorporation or intercalation, CdI_2 serves as a versatile model system for investigating low-dimensional phenomena in halide materials. It also holds significant potential for applications in photodetectors, solid-state ionics, and UV/X-ray detection technologies [32–41].

Another important direction is the study of nanostructures aimed at discovering materials with new functional properties for modern micro- and nanoelectronic devices [42–44]. Layered crystals such as CdI_2 are particularly suitable due to their atomically smooth van der Waals (vdW) surfaces, which enable the formation of molecular, organic, and metallic nanostructures and the fabrication of heterostructures via incoherent vdW epitaxy [28,45]. These surfaces also act as natural nanometrology standards for accurate characterization of nanoobjects [28,46–49].

It is known that CdI_2 develops nanoislands, nanopores, and nanoclusters under prolonged atmospheric exposure, yet the mechanisms behind these transformations and their effects on optical properties remain unclear. Existing studies suggest that such environmentally induced nanostructuring may lead to new materials for lasers, detectors, and other optoelectronic applications [49–53].

Earlier studies have shown that the surface of CdI_2 possesses unique characteristics that can be modified by controlling the conditions under which the crystals are grown and by post-processing them in different atmospheric environments [28]. By employing techniques such as atomic force microscopy (AFM) and photoluminescence (PL), it is possible to study the evolution of these surface changes and gain deeper insights into the mechanisms behind nanostructure formation and their subsequent evolution [45,54–56].

The role of ambient-induced surface transformations and their temporal development has not been systematically addressed, particularly in relation to the stability of their electronic and luminescent states. This lack of systematic insight into surface-driven transformations limits a fundamental understanding of optical ageing processes in layered halide crystals.

This study focuses on investigating the effects of prolonged exposure of CdI_2 crystals to the atmosphere on the processes of nanostructure formation. Using AFM and PL, we will explore the morphology and optical properties of these nanostructures. Furthermore, we will compare the results obtained from crystals grown from the melt versus those grown from the gas phase, in order to better understand the differences in nanocluster formation processes and their impact on the luminescence properties of the material.

2. Materials and Methods

Cadmium iodide crystals were synthesized using the Bridgman–Stockbarger method from raw materials that had undergone preliminary purification through zone melting. In the upper section of the growth ampoule, thin single-crystal plates of CdI_2 were produced via melt and gas-phase deposition [45].

For microscopic studies, samples in the form of plane-parallel plates measuring 5 mm × 5 mm and no more than 1 mm thick were cut from CdI_2 crystals along cleav-

age planes. Both the so-called "old" surfaces and freshly cleaved areas of the samples were analyzed. The "old" surfaces were formed by prolonged exposure to air, while fresh cleavage surfaces were obtained by removing the upper layers. Single-crystal CdI_2 plates grown from the gas phase were not subjected to preliminary mechanical treatment [28,55].

To examine the surface morphology and local properties of the samples, a Solver P47-PRO atomic force microscope (NT-MDT BV, Amsterdam, The Netherlands) was used. During the studies, semi-contact mode probe sensors with rectangular cantilevers of 11.8 N/m stiffness were employed. The probe tip's curvature radius did not exceed 10 nm, and the device's height resolution was 0.1 nm. AFM measurements of the micro- and nanostructure morphology were conducted in semi-contact mode [28].

3. Results and Discussion

AFM images illustrating the morphology of the van der Waals (VdW) surface of CdI_2 crystals obtained from the melt after their exposure to an air atmosphere for different durations are shown in Figure 1. The temporal evolution was investigated on the same sample, which was rigidly fixed in the microscope and covered with the protective hood supplied with the Solver P47-PRO microscope. The same surface area was examined throughout the study, as the sample was firmly mounted in the microscope and was not subjected to any mechanical disturbance during the measurements. Such experiments require dedicated laboratory time; therefore, the study was carried out on a single sample only.

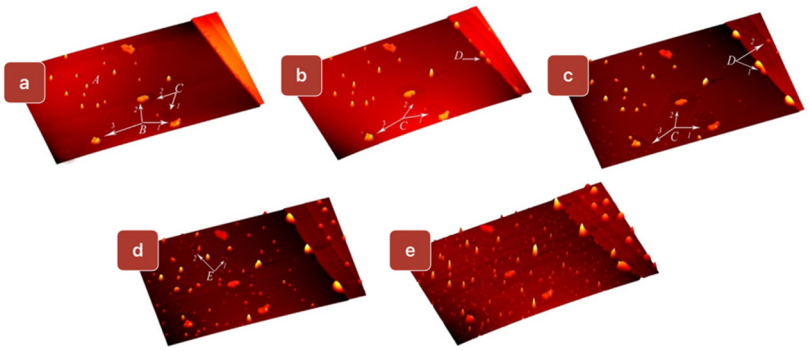

Figure 1. Time-dependent evolution of nanostructure formation on the surface of CdI_2 crystals after their exposure in air for 1 (**a**), 8 (**b**), 24 (**c**), 32 (**d**), 168 h (**e**); (area size: 6 × 10 μm; height range: (**a**) 34 nm, (**b**) 51 nm, (**c**) 55 nm, (**d**) 74 nm, (**e**) 98 nm).

Experimental conditions were as follows: ambient temperature in the range of 22–25 °C, relative humidity of 80%, atmospheric pressure of 730 mmHg. The sample was kept in air and in darkness. All AFM images were processed using the specialized Nova software provided with the Solver P47-PRO microscope.

After a short exposure time of 1 h, island-shaped nanostructures (A, B) with varying morphometric characteristics formed on the CdI_2 surface.

Nanostructures labeled as A exhibit diameters ranging from 200 to 300 nm and heights between 10 and 20 nm. In contrast, the islands labeled B (B1, B2, B3) are characterized by larger lateral dimensions but relatively smaller heights. Their average diameters reach approximately 600 nm, while their heights remain around 10 nm. The nanostructures marked in Figure 1a (B1, B2, B3) were used as reference markers, relative to which the subsequent analysis and identification of the nanostructures over time were performed.

In the vicinity of island-type nanostructures, the formation of another type of nanostructure—depressions C1 and C2 is observed. These depressions have a rounded shape, characteristic of the hexagonal atomic packing of CdI_2 (Figure 1a). The diameter of depression C1 is 473 nm, while its depth measures 0.7 nm. Given that the vertical (height)

resolution of the microscope is 0.1 nm, this value can be considered reliable and not related to crystal delamination, since the surface was not subjected to any mechanical influence during exposure to the ambient air.

After exposing the crystal to air for 8 h, the sizes of depressions C1 and C2 increased, and a new depression, C3, appeared around island B3 (Figure 1b). At the same time, the height of nanoclusters A increased by approximately 5 nm. The depth of depression C2 grew to 0.8 nm, and its diameter nearly doubled, reaching 855 nm. Additionally, new nanostructures (labeled D in Figure 1b) emerged along one of the step edges.

Following 24 h of air exposure (Figure 1c), new nanostructures appeared at the edges of depressions C1, C2, and C3, which had formed on the smooth surface, as well as on step edges B1 and B2. The height and diameter of the newly formed structures at the depression boundaries ranged from 3 to 5 nm and 100 to 120 nm, respectively. The nanostructures that developed along the step edges roughly doubled in size, reaching heights of up to 40 nm and diameters of 700 nm.

In this work, surface depressions are defined as localized height minima of at least 0.5 nm relative to the surrounding terrace, with lateral dimensions exceeding 100 nm.

In contrast, the lateral dimensions of the nanostructures formed on the smooth surface remained nearly constant. At this stage, interactions between the nanoformations were observed, leading to their coalescence and sintering into larger cluster aggregates (denoted as C in Figure 1c).

Figure 1d presents AFM images of the same surface region of CdI_2 after 32 h of air exposure. New nanoclusters appeared on the step edges, while on the smooth surface, new nanopores (E1, E2) emerged, surrounded by additional nanostructures. Simultaneously, the previously formed nanoformations continued to grow.

Nanopores here are defined as stable, approximately rounded depressions with lateral dimensions significantly exceeding those of atomic steps and persisting over time. This definition is based solely on AFM topography and does not imply a fully perforated or bulk-connected pore geometry.

After seven days (168 h) of air exposure, an ensemble of nanostructures developed across the CdI_2 surface (Figure 1e). The numerical characteristics of the nanoclusters' sizes, which form on the CdI_2 surface during prolonged exposure to an air atmosphere, are summarized in Table 1.

Table 1 is based on AFM images of the same 6 × 10 μm surface area of a single CdI_2 crystal, which was reimaged over time without moving the sample. Nanoclusters were counted using the same criteria at all stages. The observed increase in cluster number and decrease in nearest-neighbor distance therefore represent therefore time-dependent surface evolution.

To establish the growth mechanism, the temporal dynamics of the size change in the same nanocluster was studied (Table 2, Figure 2). The nanocluster analyzed in Table 2 was identified across consecutive AFM scans using its fixed position relative to step edges and neighboring nanostructures within the same surface region. The non-monotonic change in radius and volume observed at intermediate times (e.g., between 32 h and 48 h) is attributed to local surface restructuring and redistribution of material, which can temporarily modify the apparent cluster geometry without implying a change in object.

Table 1. Time dependence of the size of nanoparticles formed on the surface of CdI_2 during its exposure to air.

t, Hours	Characteristics of Clusters								
	Number	Cluster Density Per μm^2	Minimum Radius, nm	Maximum Radius, nm	Average Radius, nm	Minimum Height, nm	Maximum Height, nm	Average Height, nm	Average Distance to Nearest Neighbor, nm
8	20	0.33	38	238	92	12	34	23	922
24	37	0.62	31	253	81	4	45	20	721
32	82	1.37	31	275	79	4	57	18	474
48	81	1.35	31	240	66	9	64	23	507
54	109	1.82	31	241	58	8	62	21	434
120	143	2.38	31	234	51	8	78	23	342
144	175	2.92	31	236	49	6	77	20	309
168	344	5.73	31	258	48	6	82	18	242

Table 2. Time dependence of the size of one nanocluster.

No	*t*, Hours	Characteristics of the Nanocluster			
		Radius, nm	Area, nm^2	Height, nm	Volume, nm^3
1	1	66	353	15	1765
2	5	66	351	23	2691
3	8	73	429	29	4147
4	24	88	624	35	7280
5	29	110	976	34	11,061
6	32	117	1093	33	12,023
7	48	88	624	45	9360
8	54	82	546	47	8554
9	120	76	468	48	7488
10	144	82	546	48	8736
11	168	85	585	49	9555

At least two stages are distinguished in the time dependence of the volume of one nanocluster (Figure 2). At the first stage (0 50 h), a rapid growth of the volume is observed, which reaches a maximum at approximately 32 h. At t >100 h, a monotonic growth of the volume is observed, which is described in the $V\sqrt{t}$ coordinates by a linear dependence. This behavior is consistent with diffusion-limited growth in the late-stage regime.

For this reason, the kinetic analysis below focuses on the late-stage regime ($t \geq 100$ h), where monotonic growth is observed and phenomenological scaling can be meaningfully applied.

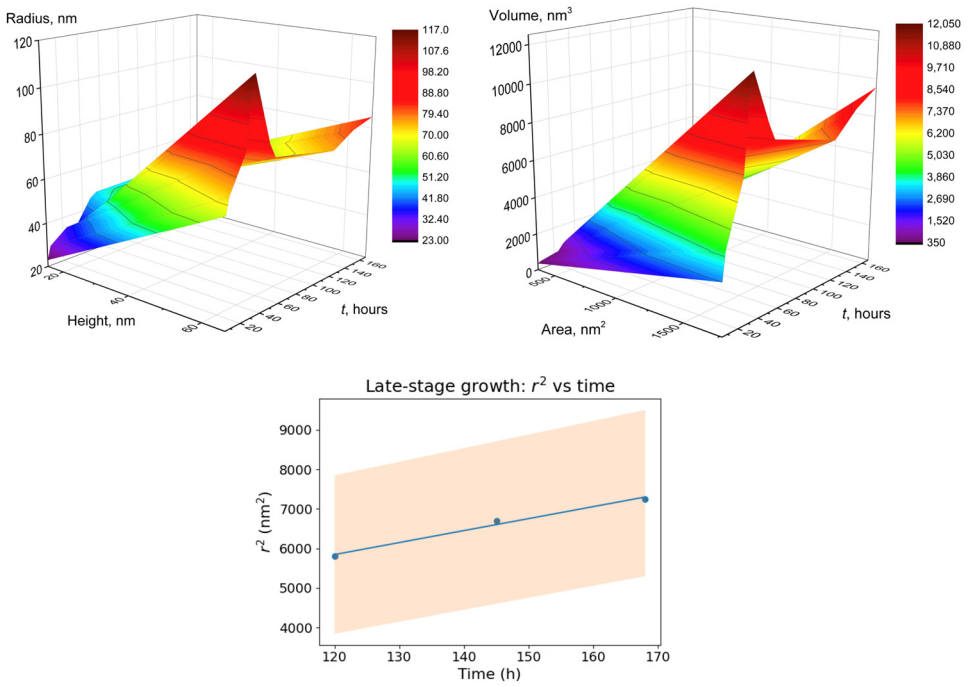

Figure 2. Time dependence of the nanocluster size parameters on the crystal exposure time in the air atmosphere (**upper panels**); late-stage growth of an individual nanocluster: r^2 as a function of exposure time (**lower panel**). The orange shaded region represents the confidence interval of the linear fit.

This stepwise formation of nanostructures highlights the dynamic processes occurring on the surface of CdI_2 crystals as they age in air, with the gradual evolution from nanopores to the development of nanoclusters. The presence of these distinct features in the AFM images further emphasizes the role of the crystal surface in the formation of nanophases and their aggregation over time.

During the initial stage of air exposure (1 h) at room temperature, island-like nanostructures begin to form on the surface. With prolonged exposure, these nanostructures progressively aggregate into nanoclusters, while the nucleation of additional nanostructures continues over time. Similarly, in CdI_2 crystals grown from the gas phase, extended air exposure exceeding 30 days results in the development of both nanopores and nanoclusters.

To determine the phase composition of nanostructures or nanoclusters obtained on the surface of CdI_2 crystals, as well as to study the chemical process of their formation, studies of the photoluminescence (PL) spectra of freshly cleaved and aged in air (over 168 h) CdI_2 crystals (grown from the melt and gas phase for comparison) were carried out. AFM analysis of CdI_2 crystals grown from the gas phase and aged in ambient air for over 30 days (Figure 3) reveals the characteristic surface morphology after long-term atmospheric exposure.

Figure 4a shows the maximum-normalized photoluminescence spectra of freshly cleaved and air-aged CdI_2 samples grown from the melt (T = 160 °C). To identify detailed features, difference spectra were constructed, revealing an intense band with a maximum at 3.1 eV, as well as several bands in the low-energy part of the spectrum with distinct maxima (Figure 4b).

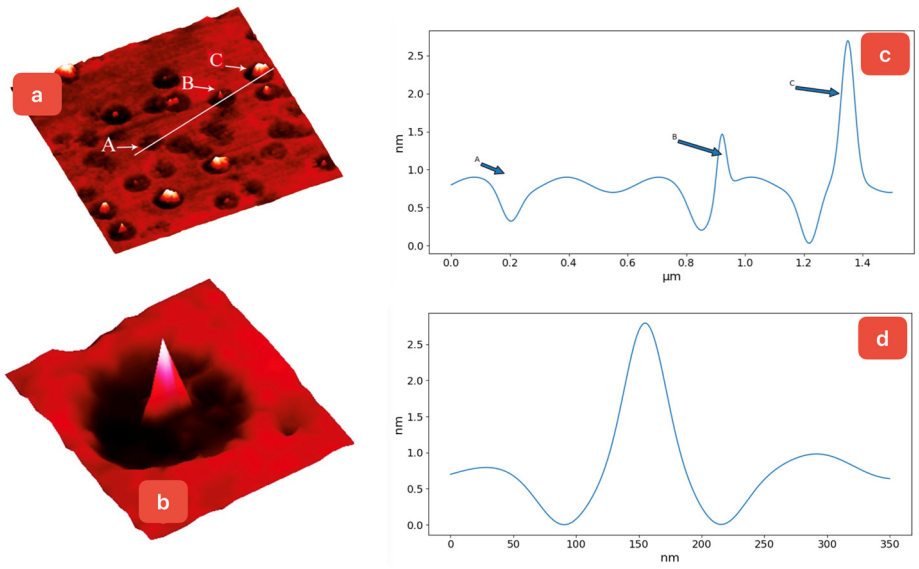

Figure 3. AFM images of the surface morphology of CdI_2 crystals grown from the gas phase, aged in an air atmosphere for a long time (30 days or more); (**a**) nanostructures: A—nanopore; B, C—nanoclusters; (**b**) nanocluster formed in a nanopore; respective profiles (**c**,**d**). Profile (**c**) is recorded along the white line shown in panel (**a**). (Area sizes: (**a**) 2 × 2 μm; (**b**) 320 × 350 nm. Height range for (**a**,**b**) is 3 nm).

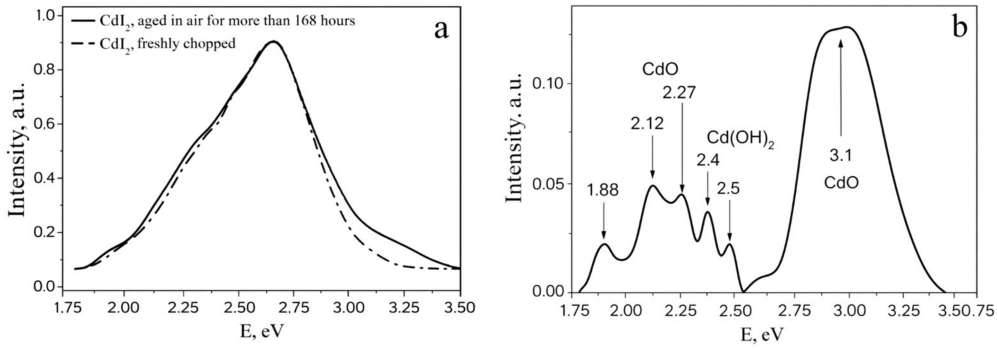

Figure 4. Photoluminescence spectra of freshly cleaved and aged in air (over 168 h) CdI_2 crystals grown from melt, T = 160 K (**a**), excitation length λ = 337 nm; (**b**) difference spectra.

By comparing the experimental difference spectra with literature data [57,58], we can associate the observed features with the luminescence of nanophases of cadmium oxide (CdO) and cadmium hydroxide ($Cd(OH)_2$). The band with a maximum at 3.1 eV (Figure 4b) corresponds to interband electronic transitions in cadmium oxide, while additional bands with maxima at 1.88, 2.12, and 2.27 eV are linked to electronic transitions to deep levels caused by defect centers [57]. The bands with maxima at 2.40 and 2.50 eV are associated with electronic transitions to deep levels in cadmium hydroxide ($Cd(OH)_2$) and interband electronic transitions in this material, respectively [58].

For comparison, Figure 5 presents the luminescence spectra of CdI_2 crystals grown from the gas phase. In addition to the intrinsic luminescence of the matrix (at 2.7 eV), a narrow band with a maximum at 2.45 eV (508 nm) is observed. As the temperature decreases, the intensity of the intrinsic luminescence increases, and its maximum shifts to the longer-wavelength region of the spectrum. However, the intensity and spectral position of the band at 508 nm remain unaffected by temperature variations. The spectral characteristics of the band with a maximum at 2.45 eV correlate well with the luminescence of CdO nanostructures [57].

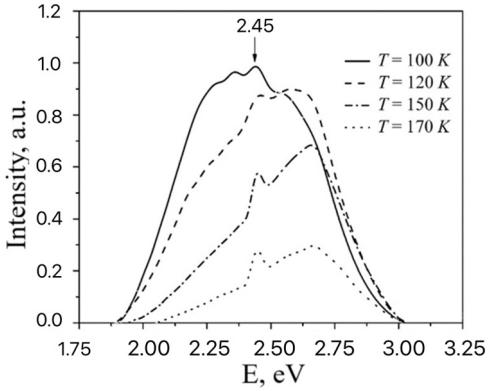

Figure 5. Temperature dependence of photoluminescence of air-aged CdI_2 crystals grown from the gas phase (measurements were carried out at 100–170 K).

Figure 6 illustrates the time evolution of the spectral luminescence of CdI_2 crystals obtained from the melt during prolonged exposure to air (e.g., 168 h and several years). In the spectra of freshly grown crystals, an intense band with a maximum around 2.48 eV (501 nm) (G-band) is observed. On the long-wavelength tail of this band, a weakly pronounced component at 2.15 eV (578 nm) (Y-band) is recorded (curve 1). The spectral composition of this luminescence is independent of the wavelength of the exciting light in the fundamental absorption region and is associated with the radiative recombination of self-localized excitons in the molecular complex $[Cd_2^{+}I_6^{2-}]_4^{-}$ [59,60].

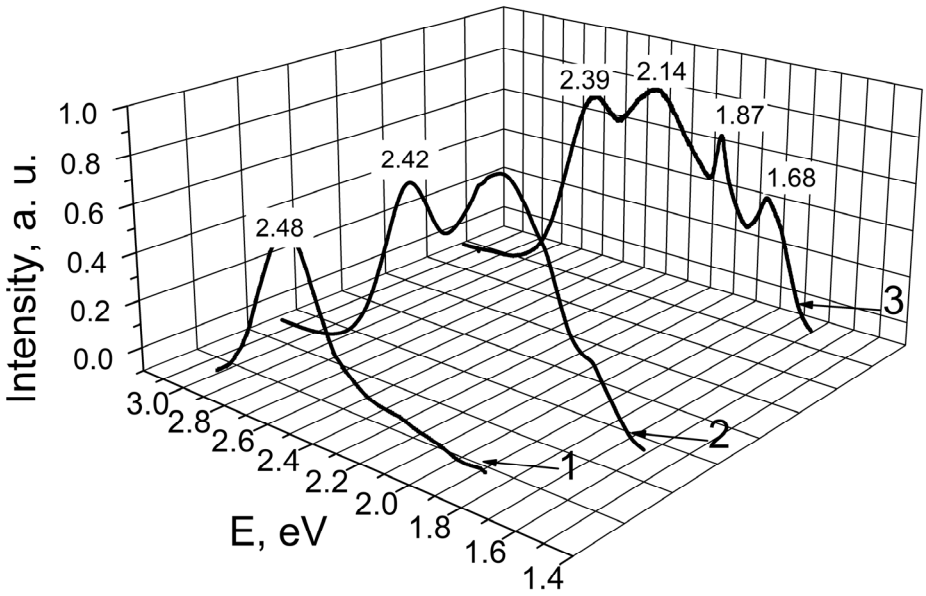

Figure 6. Luminescence spectra of freshly cleaved (curve 1) and aged in air over 186 h and over 4 years (curves 2, 3) CdI_2 crystals grown from the melt, T = 8 K (excitation length λ = 100 nm).

After prolonged exposure of the CdI_2 crystals to air, their spectra undergo significant changes. Figure 6 (curves 2 and 3) presents the spectra of CdI_2 crystals aged for more than 168 h (curve 2) and for over four years (curve 3).

Notably, both the G- and Y-bands shift to the longer-wavelength region: the maximum of the G-band moves to 2.42 eV (514 nm) (curve 2), and the maximum of the Y-band shifts to 2.04 eV (609 nm). Additionally, the intensity ratios between these bands vary, reflecting alterations in the luminescence characteristics of the aged crystals.

In a freshly grown crystal, the G-band is dominant (curve 1). However, during the aging process in air, the intensity of the Y-band becomes comparable to that of the G-band

(curves 2 and 3). It is noteworthy that similar changes were observed in the luminescence spectra of CdI_2 films after annealing at T = 420 K. In addition to the initial G-center band, intense luminescence appeared in the region around 2.2 eV (565 nm) [61].

For comparison, as CdI_2 continues to age (curve 3), a narrow band with a maximum at 1.87 eV (665 nm) appears, along with long-wavelength luminescence in the region around 1.68 eV (740 nm). The transformation of the PL spectra of CdI_2 during exposure to air, when considered alongside the AFM study results, may be linked to the formation of nanoscale structures on the surface of the crystals and their subsequent aggregation into nanoclusters.

Let us analyze the possible nature of the radiation with a maximum in the region at 1.87 eV. Its characteristic feature is a small half-width of 0.05 eV, which is significantly smaller than the half-widths of other bands (Figure 6). It appears in the spectra of CdI_2 when they are aged in air (curves 2, 3 in Figure 6), which indicates the connection of this band with nanoformations that are formed on the surface of cadmium iodide.

The phase composition of the surface nanostructures was previously identified by the authors using Raman spectroscopy [45], indicating the formation of CdO and $Cd(OH)_2$ during air exposure. The PL spectra observed here are consistent with reported emission features of these phases and thus provide complementary, but not standalone, evidence for their presence.

Now, let us consider the mechanism of formation of the cadmium hydroxide and oxide nanophases obtained. The valence of cadmium is 2 (oxidation state +2), meaning it forms two chemical bonds. These bonds are formed by two electrons from the outermost energy level of cadmium, which participate in bonding with iodine, which has 7 electrons in its outer shell. To complete its shell, iodine needs one more electron, which it "accepts" from cadmium, resulting in the formation of CdI_2.

On the other hand, cadmium possesses a vacant 5f orbital that can participate in the formation of coordination (donor–acceptor) bonds. In this case, iodine acts as the electron donor, while cadmium provides the available 5f orbital to accommodate the donated electron density.

At the edge of the I-Cd-I structural layer, the electron donor is likely to be water, specifically the oxygen atom in the water molecule. The oxygen atom has 6 electrons in its outer energy level, two of which participate in forming bonds with hydrogen to create a water molecule. The remaining four electrons can engage in the formation of a coordination bond, with cadmium acting as the acceptor through its free 5f orbital in CdI_2.

Thus, on the surface of the crystal, the first step is the coordination of water molecules. Over time, the crystal gradually undergoes hydrolysis, leading to the formation of cadmium hydroxide:

$$CdI_2 + H_2O = Cd(OH)I + HI,$$

$$Cd(OH)I + H_2O = Cd(OH)_2 + HI.$$

Since the interaction of cadmium with unsaturated (broken) bonds directly with oxygen molecules is unlikely (as cadmium in the CdI_2 compound is in the highest oxidation state of +2), it can be inferred that cadmium hydroxide serves as the "building material" for nanostructures that include cadmium oxide. This suggests that the formation of cadmium hydroxide on the crystal surface might be a precursor step in the creation of cadmium oxide nanophases, where the hydroxide undergoes further transformation or dehydration to form cadmium oxide structures ($Cd(OH)_2 = CdO + H_2O$).

Before moving on to the conclusion, it is necessary to note that the results of this work are of particular interest for a more in-depth study of similar processes in other promising halides [62–77], that have gained new interest for light detection and imaging.

4. Conclusions

The time evolution of nanoscale structure formation on the surfaces of CdI_2 crystals grown from the melt and from the gas phase was investigated. The AFM method revealed that at the initial stages of keeping the samples in an air atmosphere (for 1 h) at room temperature, island-shaped nanostructures begin to form. With increasing exposure time, these structures undergo aggregation and eventually form nanoclusters, while the persistence of nanostructure formation continues. This process of nanostructure development is observed both in CdI_2 crystals grown from the melt and in those grown from the gas phase. In particular, for the gas-phase-grown crystals, after exposure to air for more than 30 days, nanopores and nanoclusters are observed to form on the surface.

Photoluminescence spectroscopy further confirms the composition of these formed nanoclusters, showing that they contain cadmium hydroxide ($Cd(OH)_2$) and cadmium oxide (CdO). The formation of these nanostructures plays a crucial role in the time evolution of the low-temperature luminescence spectra of CdI_2 crystals. Additional luminescence bands with maxima at 1.87 eV and a long-wavelength emission near 1.68 eV emerge during air ageing. These features indicate the appearance of new electronic transitions associated with the evolving surface of nanostructures. This suggests a dynamic relationship between the structural evolution of the material and its optical properties over time.

Author Contributions: Writing—original draft preparation, I.R.; writing—review and editing, H.K., I.K. and A.I.P.; validation, I.R. and I.K.; funding acquisition, M.K., N.K. and A.I.P.; investigation, I.R., H.K., I.K., M.K., N.K. and A.I.P.; software, I.R., H.K. and I.K.; supervision, H.K., M.K., N.K. and A.I.P. All authors have read and agreed to the published version of the manuscript.

Funding: This research was funded by Ministry of Education and Science of Ukraine for providing support (Projects No 0125U001883 and 0125U003462), Latvian research project lzp-2023/1-0453, Latvian State Research Program No. VPP-IZM-CERN-2022/1-0001 and Estonian Ministry of Education and Research (TK210).

Data Availability Statement: The original contributions presented in this study are included in the article. Further inquiries can be directed to the corresponding authors.

Acknowledgments: Authors (I.R.; H.K. and I.K.) would like to thank the Ministry of Education and Science of Ukraine for providing support (Projects No 0125U001883 and 0125U003462). In addition, Marina Konuhova and Anatoli I. Popov were supported by Latvian research project lzp-2023/1-0453, "Prediction of long-term stability of functional materials under extreme radiation conditions", and the Latvian State Research Program No. VPP-IZM-CERN-2022/1-0001. Finally, research of N.K. was supported by Estonian Ministry of Education and Research (TK210).

Conflicts of Interest: The authors declare no conflicts of interest.

References

1. Lushchik, A.; Lushchik, C.; Vasil'chenko, E.; Popov, A.I. Radiation Creation of Cation Defects in Alkali Halide Crystals: Review and Today's Concept. *Low Temp. Phys.* **2018**, *44*, 269–277. [CrossRef]
2. Vaněček, V.; Děcká, K.; Mihóková, E.; Čuba, V.; Král, R.; Nikl, M. Advanced Halide Scintillators: From the Bulk to Nano. *Adv. Photon. Res.* **2022**, *3*, 2200011. [CrossRef]
3. Chen, H. Scintillation Mechanisms in Inorganic Scintillators: An Excitonic and Alkali Halides Focused Review. In *Hard X-Ray, Gamma-Ray, and Neutron Detector Physics XXIV*; SPIE: Bellingham, WA, USA, 2022; Volume 12241, pp. 12–30.
4. Racu, A.V.; Ristić, Z.; Ćirić, A.; Đorđević, D.; Bușe, G.; Poienar, M.; Gutmann, M.J.; Ivashko, O.; Ștef, M.; Vizman, D.; et al. Analysis of Site Symmetries of Er^{3+}-Doped CaF_2 and BaF_2 Crystals by High-Resolution Photoluminescence Spectroscopy. *Opt. Mater.* **2023**, *136*, 113337. [CrossRef]
5. Levkovets, S.I.; Khyzhun, O.Y.; Myronchuk, G.L.; Fochuk, P.M.; Piasecki, M.; Kityk, I.V.; Fedorchuk, A.O.; Levkovets, V.I.; Parasyuk, L.V. Synthesis, Electronic Structure and Optical Properties of $PbBr_{1.2}I_{0.8}$. *J. Electron Spectrosc. Relat. Phenom.* **2017**, *218*, 13–20. [CrossRef]

6. Nicoara, I.; Ștef, M.; Vizman, D.; Negut, C.D. Gamma-Rays Induced Color Centers in Pb^{2+}-Doped CaF_2 Crystals. *Radiat. Phys. Chem.* **2018**, *153*, 70–78. [CrossRef]
7. Popov, A.I.; Elsts, E.; Kotomin, E.A.; Moskina, A.; Karipbayev, Z.T.; Makarenko, I.; Pazylbek, S.; Kuzovkov, V.K. Thermal Annealing of Radiation Defects in MgF_2 Single Crystals Induced by Neutrons at Low Temperatures. *Nucl. Instrum. Methods Phys. Res. B* **2020**, *480*, 16–21. [CrossRef]
8. Shunkeyev, K.; Tilep, A.; Sagimbayeva, S.; Lushchik, A.; Ubaev, Z.; Myasnikova, L.; Zhanturina, N.; Aimaganbetova, Z. The Enhancement of Exciton-Like Luminescence in KCl Single Crystals under Local and Uniaxial Elastic Lattice Deformation. *Nucl. Instrum. Methods Phys. Res. B* **2022**, *528*, 20–26. [CrossRef]
9. Lushchik, C.; Kolk, J.; Lushchik, A.; Lushchik, N.; Taiirov, M.; Vasilchenko, E. Decay of excitons into long-lived F, H and α, I pairs in KCl. *Phys. Status Solidi B* **1982**, *114*, 103–111. [CrossRef]
10. Shunkeyev, K.; Aimaganbetova, Z.; Myasnikova, L.; Maratova, A.; Ubaev, Z. Mechanisms of Radiation Defect Formation in KCl Crystals under the Influence of Local and Plastic Deformation. *Nucl. Instrum. Methods Phys. Res. B* **2021**, *509*, 7–11. [CrossRef]
11. Myasnikova, L.N.; Istlyaup, A.S.; Sergeyev, D.M.; Shunkeyev, K.S. Computer Simulations of the Band Structure and Density of States of the Linear Chains of NaCl Ions. *Latv. J. Phys. Tech. Sci.* **2019**, *56*, 49–56. [CrossRef]
12. Tariwong, Y.; Kim, H.J.; Quang, N.D.; Khan, A.; Daniel, D.J.; Limsuwan, P.; Wantana, N.; Pakawanit, P.; Vittayakorn, N.; Intachai, N.; et al. Ca Co-Doped CsI(Tl) Crystal Scintillator for γ- and X-Ray Detecting Applications. *Radiat. Phys. Chem.* **2025**, *226*, 112241. [CrossRef]
13. Romanova, M.; Chertopalov, S.; Dekhtyar, Y.; Fekete, L.; Lančok, J.; Novotný, M.; Pokorný, P.; Popov, A.I.; Sorokins, H.; Vilken, A. Charge Trapping in SiO_2 Substrate during Electron Beam Deposition of CaF_2 Thin Films of Different Thicknesses. *Opt. Mater. X* **2025**, *25*, 100400. [CrossRef]
14. Ubukata, T.; Otake, S.; Kato, T.; Nakauchi, D.; Kawaguchi, N.; Yanagida, T. Scintillation Properties of $SrCl_2$:Eu Transparent Ceramics Fabricated by Spark Plasma Sintering Method. *J. Lumin.* **2025**, *278*, 121021. [CrossRef]
15. Kalniņš, A.; Pļaviņa, I.; Popov, A.I.; Tāle, A. Determination of the effective absorption cross-section of F-centres in KBr–In by photostimulated luminescence. *Phys. Status Solidi B* **1990**, *161*, 85–89. [CrossRef]
16. Zheng, B.; Deng, L.; Ma, H.; Wang, J.; Yao, Y.; Qi, D.; Shen, Y.; Sun, Z.; Zhang, S. Defect-related luminescence in BaF_2 nanoparticles for plant cell imaging. *Appl. Phys. Lett.* **2025**, *126*, 173701. [CrossRef]
17. Popov, A.I. Manifestation of H-Centre Aggregation in the Exciton-Induced Thermostimulated Luminescence of KBr:In and KBr:Tl Crystals. *Phys. Status Solidi B* **1992**, *169*, K47–K51. [CrossRef]
18. Rogulis, U.; Spaeth, J.-M.; Elsts, E.; Dolgopolova, A. Tl-related radiation defects in CsI:Tl. *Radiat. Meas.* **2004**, *38*, 389–392. [CrossRef]
19. Ronda, C.R.; Zwaal, E.; Folkersma, H.F.; Lenselink, A.; Haas, C. Absorption and luminescence of photochromic CdI_2:CuI. *J. Solid State Chem.* **1988**, *72*, 80–91. [CrossRef]
20. Xu, Z.; Rui, Q.; Geng, Y.; Li, J.; Wang, Q.; Wang, X. Pressure-induced decomposition of cadmium iodide. *EPL (Europhys. Lett.)* **2022**, *140*, 16003. [CrossRef]
21. Miah, M.I. Size- and temperature-dependent second-order optical effects in copper-doped cadmium iodide nanocrystals. *J. Appl. Phys.* **2008**, *104*, 064313. [CrossRef]
22. Wang, W.; Qiao, J.; Wang, L.; Duan, L.; Zhang, D.; Yang, W.; Qiu, Y. Synthesis, structures, and optical properties of cadmium iodide/phenethylamine hybrid materials with controlled structures and emissions. *Inorg. Chem.* **2007**, *46*, 10252–10260. [CrossRef]
23. Yue, L.; Jin, W.; Mao, A.J.; Kuang, X. Single-layer MX_2 (M = Zn, Cd; X = Cl, I): Auxetic semiconductors with strain-tunable optoelectronic properties. *J. Phys. Chem. C* **2021**, *125*, 12983–12990. [CrossRef]
24. Tao, L.; Huang, L. Computational design of enhanced photocatalytic activity of two-dimensional cadmium iodide. *RSC Adv.* **2017**, *7*, 53653–53657. [CrossRef]
25. Tubbs, M.R. Polytypism and spiral growth in cadmium iodide. *Acta Cryst. B* **1971**, *27*, 857–859. [CrossRef]
26. Aldwayyan, A.S.; Al-Jekhedab, F.M.; Al-Noaimi, M.; Hammouti, B.; Hadda, T.B.; Suleiman, M.; Warad, I. Synthesis and characterization of CdO nanoparticles starting from organometallic dmphen-CdI_2 complex. *Int. J. Electrochem. Sci.* **2013**, *8*, 10506–10514. [CrossRef]
27. Bolesta, I.; Velgosh, S.; Datsiuk, Y.; Karbovnyk, I.; Lesivtsiv, V.; Kulay, T.; Popov, A.I.; Bellucci, S.; Cestelli Guidi, M.; Marcelli, A.; et al. Optical, infrared and electron-microscopy studies of (Cdi)n metallic clusters in layered CdI_2 crystals. *Radiat. Meas.* **2007**, *42*, 851–854. [CrossRef]
28. Bolesta, I.M.; Rovetskyj, I.N.; Partyka, M.V.; Karbovnyk, I.D.; Kulyk, B.Y. Formation of nanostructures on the VdW-surface of CdI_2 crystals. *Ukr. J. Phys.* **2013**, *58*, 490. [CrossRef]
29. Miah, M.I. Stimulated photoluminescence and optical limiting in CdI_2. *Opt. Mater.* **2002**, *20*, 279–282. [CrossRef]
30. Miah, M.I. One-, two-, and three-photon processes in CdI_2 crystal. *Opt. Mater.* **2004**, *25*, 353–357. [CrossRef]
31. Miah, M.I. Multiphoton excitation and thermal activation in indirect bandgap semiconductors. *Opt. Quantum Electron.* **2018**, *50*, 355. [CrossRef]

32. Novosad, S.S.; Matviishin, I.M.; Novosad, I.S.; Novosad, O.S. Spectral and kinetic characteristics of CdI_2 and CdI_2:Pb scintillators. *J. Appl. Spectrosc.* **2008**, *75*, 826–831. [CrossRef]
33. Bukivskii, A.P.; Gnatenko, Y.P.; Piryatinski, Y.P.; Fesych, I.V.; Lendel, V.V.; Tkach, V.M.; Bukivskij, P.M. Nature of radiative recombination processes in layered heterogeneous $PbCdI_2$ thick films: Promising scintillator materials. *Adv. Condens. Matter Phys.* **2018**, *2018*, 2762369. [CrossRef]
34. Salakhutdinov, G.K.; Efanov, D.V. Nonlinear effects in scintillation detectors. *Instrum. Exp. Tech.* **2015**, *58*, 345–349. [CrossRef]
35. Chen, C. The electronic and optical properties of Cu-doped CdI_2. *Optik* **2013**, *124*, 3230–3234. [CrossRef]
36. Rybak, O.V.; Chekaylo, M.V.; Pokladok, N.T. Vapor phase growth and properties of mixed layered $Pb_{1-x}Cd_xI_2$ semiconductors. *Phys. Chem. Solid State* **2022**, *23*, 311–316. [CrossRef]
37. Novosad, S.S.; Novosad, I.S.; Goncharuk, V.E. Recombination processes in europium-doped cadmium iodide crystals. *J. Appl. Spectrosc.* **2009**, *76*, 334–340. [CrossRef]
38. Novosad, I.; Kalivoshka, B.; Novosad, S.; Vas'kiv, A. Effect of preparation conditions and impurities on the spectral characteristics of cadmium iodide. In Proceedings of the XIth International Scientific and Practical Conference on Electronics and Information Technologies (ELIT), Lviv, Ukraine, 16–18 September 2019; pp. 291–294. [CrossRef]
39. Cummings, T.; Marín, C.; Ostrogorsky, A.G.; Burger, A.; Bliss, M. Tetragonal red and yellow HgI_2-CdI_2 crystals for X- and γ-ray solid-state detectors directionally solidified under argon pressure of 20 atm. *J. Cryst. Growth* **2006**, *297*, 334–338. [CrossRef]
40. Furyer, M.S.; Skubenko, P.A.; Bukivskij, P.M.; Tarakhan, L.M.; Chesnokov, E.D.; Vertegel, I.G.; Ovcharenko, A.I.; Ivanova, L.S.; Gamernyk, R.V.; Gnatenko, Y.P. Study of the photoluminescence and photoelectric properties of $Pb_{1-x}Cd_xI_2$ alloys. *J. Appl. Phys.* **2010**, *108*, 103711. [CrossRef]
41. Bukivskii, A.P.; Gnatenko, Y.P.; Piryatinskii, Y.P.; Gamernyk, R.V. Nature of radiative recombination processes in layered semiconductor $PbCdI_2$ nanostructural scintillation material. *J. Lumin.* **2017**, *185*, 83–91. [CrossRef]
42. Momin, M.A.; Islam, M.A.; Nesa, M.; Sharmin, M.; Rahman, M.J.; Bhuiyan, A.H. Effect of M (Ni, Cu, Zn) Doping on the Structural, Electronic, Optical, and Thermal Properties of CdI_2: DFT-Based Theoretical Studies. *AIP Adv.* **2021**, *11*, 055012. [CrossRef]
43. Karbovnyk, I.; Bolesta, I.; Rovetskyi, I.; Lesivtsiv, V.; Shmygelsky, Y.; Velgosh, S.; Popov, A.I. Long-Term Evolution of Luminescent Properties in CdI_2 Crystals. *Low Temp. Phys.* **2016**, *42*, 594–596. [CrossRef]
44. Karbovnyk, I.; Bolesta, I.; Rovetskii, I.; Velgosh, S.; Klym, H. Studies of CdI_2–Bi^{3+} Microstructures with Optical Methods, Atomic Force Microscopy and Positron Annihilation Spectroscopy. *Mater. Sci. Pol.* **2014**, *32*, 391–395. [CrossRef]
45. Bolesta, I.M.; Rovetskii, I.N.; Karbovnik, I.D.; Rykhlyuk, S.V.; Partyka, M.V.; Gloskovskaya, N.V. Formation and Optical Properties of CdI_2 Nanostructures. *J. Appl. Spectrosc.* **2015**, *82*, 84–90. [CrossRef]
46. Ai, R.; Guan, X.; Li, J.; Yao, K.; Chen, P.; Zhang, Z.; Duan, X. Growth of Single-Crystalline Cadmium Iodide Nanoplates, CdI_2/MoS_2 (WS_2, WSe_2) van der Waals Heterostructures, and Patterned Arrays. *ACS Nano* **2017**, *11*, 3413–3419. [CrossRef] [PubMed]
47. Bellucci, S.; Bolesta, I.; Guidi, M.C.; Karbovnyk, I.; Lesivtsiv, V.; Micciulla, F.; Pastore, R.; Popov, A.I.; Velgosh, S. Cadmium Clusters in CdI_2 Layered Crystals: The Influence on the Optical Properties. *J. Phys. Condens. Matter* **2007**, *19*, 395015. [CrossRef]
48. Bellucci, S.; Bolesta, I.; Karbovnyk, I.; Hrytskiv, R.; Fafilek, G.; Popov, A.I. Microstructure of Ag_2BI_4 (B = Ag, Cd) Superionics Studied by SEM, Impedance Spectroscopy and Fractal Dimension Analysis. *J. Phys. Condens. Matter* **2008**, *20*, 474211. [CrossRef]
49. Ueno, T.; Yamamoto, H.; Saiki, K.; Koma, A. Van der Waals Epitaxy of Metal Dihalide. *Appl. Surf. Sci.* **1997**, *113*, 33–37. [CrossRef]
50. Kumari, S.; Suthar, D.; Himanshu; Kumari, N.; Dhaka, M.S. Understanding Grain Growth Mechanism in Vacuum Evaporated CdTe Thin Films by Different Halide Treatments: An Evolution of Ion Size Impact on Physical Properties for Solar Cell Applications. *Comments Inorg. Chem.* **2023**, *43*, 429–464. [CrossRef]
51. Roccanova, R.; Ming, W.; Whiteside, V.R.; McGuire, M.A.; Sellers, I.R.; Du, M.H.; Saparov, B. Synthesis, Crystal and Electronic Structures, and Optical Properties of $(CH_3NH_3)_2CdX_4$ (X = Cl, Br, I). *Inorg. Chem.* **2017**, *56*, 13878–13888. [CrossRef]
52. Suchikova, Y.; Nazarovets, S.; Popov, A.I. Ga_2O_3 Solar-Blind Photodetectors: From Civilian Applications to Missile Detection and Research Agenda. *Opt. Mater.* **2024**, *142*, 116397. [CrossRef]
53. Suchikova, Y.; Kovachov, S.; Bohdanov, I.; Popova, E.; Moskina, A.; Popov, A.I. Characterization of CdxTeyOz/CdS/ZnO Heterostructures Synthesized by the SILAR Method. *Coatings* **2023**, *13*, 639. [CrossRef]
54. Gal'chinskii, A.V.; Gloskovskaya, N.V.; Yaritskaya, L.I. Carrier Trapping and Delocalization in PbI_2-Containing CdI_2 Crystals. *Inorg. Mater.* **2012**, *48*, 423–427. [CrossRef]
55. Bolesta, I.M.; Rovetskii, I.N.; Velgosh, S.R.; Rykhlyuk, S.V.; Karbovnyk, I.D.; Gloskovskaya, N.V. Morphology and Optical Properties of Nanostructures Formed in Non-Stoichiometric CdI_2 Crystals. *Ukr. J. Phys.* **2018**, *63*, 816. [CrossRef]
56. Bolesta, I.M.; Gloskovskaya, N.V.; Panasyuk, M.R.; Rovetskii, I.N.; Yaritskaya, L.I. Extrinsic Luminescence Centers in CdI_2 Crystals Doped with PbI_2 (10^{-4} to 1 mol%). *Inorg. Mater.* **2013**, *49*, 214–218. [CrossRef]
57. Benhaliliba, M.; Benouis, C.E.; Tiburcio-Silver, A.; Yakuphanoglu, F.; Avila-Garcia, A.; Tavira, A.; Mouffak, Z. Luminescence and Physical Properties of Copper Doped CdO Derived Nanostructures. *J. Lumin.* **2012**, *132*, 2653–2658. [CrossRef]

58. Sahraei, R.; Mihandoost, A.; Nabiyouni, G.; Daneshfar, A.; Roushani, M.; Majles Ara, M.H. Room Temperature Synthesis and Characterization of Ultralong $Cd(OH)_2$ Nanowires: A Simple and Template-Free Chemical Route. *Appl. Phys. A* **2012**, *109*, 471–475. [CrossRef]
59. Matsumoto, H.; Nakagawa, H. Relaxed Excitonic States in CdI_2 Crystals. *J. Lumin.* **1979**, *18*, 19–22. [CrossRef]
60. Kawabata, S.; Nakagawa, H. Life-Time Resolved Emission Spectra in CdI_2 Crystals. *J. Lumin.* **2007**, *126*, 48–52. [CrossRef]
61. Fukui, K.; Asakura, K.; Niimi, K.I.; Ishizue, I.; Nakagawa, H. Absorption and Luminescence Spectra of Amorphous CdI_2 Thin Films. *J. Electron Spectrosc. Relat. Phenom.* **1999**, *101*, 299–302. [CrossRef]
62. Zhunusbekov, A.M.; Strelkova, A.V.; Karipbayev, Z.T.; Kumarbekov, K.K.; Akilbekov, A.; Kassymkhanova, R.N.; Kassymzhanov, M.T.; Smortsova, Y.; Popov, A.I. Luminescence Investigation of $BaMgF_4$ Ceramics under VUV Synchrotron Excitation. *Crystals* **2025**, *15*, 127. [CrossRef]
63. Nagorny, S. Novel Cs_2HfCl_6 Crystal Scintillator: Recent Progress and Perspectives. *Physics* **2021**, *3*, 320–351. [CrossRef]
64. Buryi, M.; Kral, R.; Babin, V.; Paterek, J.; Vanecek, V.; Veverka, P.; Kohoutkova, M.; Laguta, V.; Fasoli, M.; Villa, I.; et al. Trapping and Recombination Centers in Cesium Hafnium Chloride Single Crystals: EPR and TSL Study. *J. Phys. Chem. C* **2019**, *123*, 19402–19411. [CrossRef]
65. Maji, S.B.; Vanetsev, A.; Mändar, H.; Nagirnyi, V.; Chernenko, K.; Kirm, M. Investigation of Luminescence Properties of Hydrothermally Synthesized Pr^{3+}-Doped $BaLuF_5$ Nanoparticles under Excitation by VUV Photons. *Opt. Mater.* **2024**, *154*, 115781. [CrossRef]
66. Saaring, J.; Vanetsev, A.; Chernenko, K.; Feldbach, E.; Kudryavtseva, I.; Mändar, H.; Pikker, S.; Pärna, R.; Nagirnyi, V.; Omelkov, S.; et al. Time-Resolved Luminescence Spectroscopy of Ultrafast Emissions in $BaGeF_6$. *J. Lumin.* **2022**, *244*, 118729. [CrossRef]
67. Saaring, J.; Vanetsev, A.; Chernenko, K.; Feldbach, E.; Kudryavtseva, I.; Mändar, H.; Pärna, R.; Nagirnyi, V.; Omelkov, S.; Romet, I.; et al. Relaxation of Electronic Excitations in K_2GeF_6 Studied by Means of Time-Resolved Luminescence Spectroscopy under VUV and Pulsed Electron Beam Excitation. *J. Alloys Compd.* **2021**, *883*, 160916. [CrossRef]
68. Cirulis, J.; Antuzevics, A.; Fedotovs, A.; Rogulis, U.; Zvejnieks, G. Local Structure of an Oxygen Impurity and Fluorine Vacancy Complex in $LiYF_4$. *Materialia* **2023**, *30*, 101848. [CrossRef]
69. Antuzevics, A.; Fedotovs, A.; Berzins, D.; Rogulis, U.; Auzins, K.; Zolotarjovs, A.; Baldochi, S.L. Recombination Luminescence of X-Ray Induced Paramagnetic Defects in BaY_2F_8. *J. Lumin.* **2020**, *223*, 117216. [CrossRef]
70. Li, X.; Hu, C.; Guo, L.; Ye, J.; Zhang, Y.; Xu, J.; Wu, J.; Liu, Q.; Shi, Y.; Chen, J.; et al. Scintillation properties and slow component suppression mechanism of BaF_2 transparent ceramics. *J. Am. Ceram. Soc.* **2025**, *108*, e20469. [CrossRef]
71. Ubukata, T.; Otake, S.; Kimura, H.; Kato, T.; Nakauchi, D.; Kawaguchi, N.; Yanagida, T. Effect of Eu-doping on optical and scintillation properties of $CaCl_2$ transparent ceramics. *J. Mater. Sci. Mater. Electron.* **2025**, *36*, 2240. [CrossRef]
72. Okazaki, K.; Koshimizu, M.; Koba, Y.; Kato, T.; Nakauchi, D.; Kawaguchi, N.; Yanagida, T. Effects of linear energy transfer on thermoluminescence properties of Eu-doped CaF_2 ceramics. *Nucl. Instrum. Methods Phys. Res. B* **2025**, *566*, 165785. [CrossRef]
73. Wauke, T.; Kawano, N.; Kato, T.; Takebuchi, Y.; Fukushima, H.; Okada, G.; Yanagida, T. Dosimetric properties of Eu-doped Ca_2BO_3Cl. *Nucl. Instrum. Methods Phys. Res. B* **2024**, *548*, 165227. [CrossRef]
74. Stef, M.; Buse, G.; Gutmann, M.; Poienar, M. Structural and optical properties of 5 mol% ErF_3-doped fluoride crystals. *Phys. Scr.* **2025**, *100*, 105902. [CrossRef]
75. Ćirić, A.; Stef, M.; Buse, G.; Periša, J.; Ristić, Z.; Gavrilović, T.; Dramićanin, M.D. Principal component analysis luminescence thermometry of Ce^{3+}: Case study of BaF_2:Ce^{3+} single crystals. *J. Appl. Cryst.* **2025**, *58*, 1659–1664. [CrossRef]
76. Stef, M.; Schornig, C.; Buse, G. Optical and Dielectric Properties of BaF_2:(Er,Yb) Co-Doped Crystal. *Materials* **2025**, *18*, 1915. [CrossRef] [PubMed]
77. Schornig, C.; Stef, M.; Buse, G.; Poienar, M.; Veber, P.; Vizman, D. Spectroscopic Properties of TmF_3-Doped CaF_2 Crystals. *Materials* **2024**, *17*, 4965. [CrossRef] [PubMed]